remote sensing

MDPI

Article

The Spatial-Temporal Distribution of GOCI-Derived Suspended Sediment in Taiwan Coastal Water Induced by Typhoon Soudelor

Pham Minh Chau [1,2], Chi-Kuei Wang [1,*] and An-Te Huang [1]

[1] Department of Geomatics, National Cheng Kung University, No. 1 University Road, East District, Tainan City 701, Taiwan; chaupm.ctt@vimaru.edu.vn (P.M.C.); end7879520@gmail.com (A.-T.H.)

[2] Department of Civil Engineering, Vietnam Maritime University, 484 Lach Tray Street, Haiphong City 180000, Vietnam

* Correspondence: chikuei@ncku.edu.tw; Tel.: +886-6-275-7575 (ext. 63825)

Abstract: This paper discusses the use of a Geostationary Ocean Color Imager (GOCI) to monitor the spatial–temporal distribution of suspended sediment (SS) along the coastal waters of northern Taiwan which was affected by Typhoon Soudelor from 8 to 10 August 2015. High temporal resolution satellite images derived from GOCI were processed to generate four-day average images of SS for pre- and post-typhoon periods. By using these four-day average images, characteristics of SS along the north of Taiwan coastal water can be tracked. The results show that SS concentration increased in the four-day average image immediately after the typhoon (11–14 August), and then decreased in the four-day average image 9 to 12 days after the typhoon (19–22 August). The mouths of the Dajia River and Tamsui River were hotspots of SS, ranging from 9 to 15 g/m^3 during the two post-typhoon periods. Moreover, the maximum suspended sediment (SS_{max}) and its corresponding time (t_{max}) can be computed using GOCI hourly images for the post-typhoon period from 08:30 on 11 August to 08:30 on 22 August. The results show that SS_{max} occurred in the west coastal water within 4 days post-typhoon, and SS_{max} occurred in the east coastal water 9 to 12 days post-typhoon. Furthermore, an exponential decay model was used to compute the time when 90% of typhoon-induced SS was dissipated after Typhoon Soudelor (t_{90}). It was found that t_{90} in the mouths of the Tamsui River and Heping River was the longest among all coastal waters of our study area, with a range of 360–480 h. River discharge and ocean currents with suspended sediment concentration are discussed.

Keywords: GOCI; suspended sediment; Typhoon Soudelor; spatial–temporal distribution

Citation: Chau, P.M.; Wang, C.-K.; Huang, A.-T. The Spatial-Temporal Distribution of GOCI-Derived Suspended Sediment in Taiwan Coastal Water Induced by Typhoon Soudelor. *Remote Sens.* **2021**, *13*, 194. https://doi.org/10.3390/rs13020194

Received: 6 November 2020
Accepted: 5 January 2021
Published: 8 January 2021

1. Introduction

Suspended sediment (SS) is a key part of studying shallow waters, such as coastal regions, because of its influence on the marine environment and ecosystems [1]. Therefore, monitoring the characteristics of SS can aid in better understanding the bio-geomorphological processes and validate spatially distributed hydrodynamic and transport models in coastal water regions [2]. There are many monitoring methods, such as in situ measurements with a cruise, station observations, numerical models, remote sensing, etc. In situ measurements with a cruise, numerical models, and station observations are costly and time-consuming [3,4]. Remote sensing provides a viable solution for monitoring SS in coastal waters because it can cover large areas at the same time. Moreover, compared with other methods, satellite images also offer richer spatial information and can overcome operational cost issues due to state-of-the-art technologies. For example, the first geostationary ocean color observation satellite has been used for coastal water turbidity and Sentinel-3 missions for scientific observations of the ocean [5,6].

Many regions around the world are affected by tropical storms, including Taiwan. Typhoon-induced suspended sediment (SS) in the coastal water region has an impact on the marine environment. For instance, Typhoon Morakot had an influence on the marine environment in the East China Sea inner shelf and Okinawa Trough [7,8]. The heavy rains and episodic cyclones associated with typhoons increase the total suspended sediment, sea surface temperature, and phytoplankton. In addition, the high waves and strong wind speeds of typhoons, inducing re-suspension of bottom sediments, have been discussed [9]. The ocean surface current related to Hurricane Sandy, Typhoon Morakot, and Typhoon Saola caused the spreading of suspended sediments from the coast to the open sea [10–12]. No previous studies have used remote sensing to investigate the spatiotemporal distribution of suspended sediment in Taiwan coastal waters, induced by a typhoon. We used satellite images to do this in the north of Taiwan.

Several international studies have used satellite images to assess sediment in coastal water regions. For example, remote sensing has been used to assess typhoon-induced SS concentrations. In Apalachicola Bay, Florida, USA, observations of typhoon-induced SS were conducted by using 250 m Terra MODIS (Moderate Resolution Imaging Spectroradiometer) images during Hurricane Frances [13]. The impact of Typhoon Saomai on SS concentration in the East China Sea was calculated using Aqua and Terra MODIS images [14]. Combinations of multi-satellite images (including MODIS, MERIS (the Medium Resolution Imaging Spectrometer), and GOCI) were used to show the dynamics of suspended sediment associated with Typhoon Tembin in the East China Sea [15]. The sediment transport in the Taiwan Strait induced by Typhoons Soulik and Morakot has been monitored by using Aqua MODIS images [16,17]. The spatial–temporal distribution of SS has not yet been considered because of the limitation of quality data under typhoons. Therefore, this paper tries to bridge the gap between the spatial–temporal distribution of SS induced by a typhoon and data limitations.

The Geostationary Ocean Color Imager (GOCI), a satellite sensor, can overcome the limitation of quality data under typhoon weather conditions due to its temporal resolution [18]. The GOCI is operated by the Korea Ocean Satellite Center (KOSC) at the Korea Institute of Ocean Science and Technology (KIOST). It is the first ocean color satellite placed in geostationary orbit to provide eight hourly images during the daytime (from 08:30 to 15:30 local time at one-hour intervals) with a spatial resolution of 500 m. GOCI covers about 2500 km $\times$ 2500 km centering on the Korean Peninsula (at the center of 130° E, 36° N), including the north of Taiwan. It has six visible bands from 412 to 680 nm and two near-infrared bands at 745 and 865 nm. The bands at wavelengths of 555 and 660 nm are used for suspended sediment extraction [19–22]. All of the existing studies related to GOCI-derived suspended sediment focused on monitoring the temporal variation of water turbidity and the diurnal dynamics of suspended sediment in coastal water. For instance, GOCI hourly images have been used to monitor the diurnal and seasonal variability of suspended sediment concentration in a macro-tidal estuary [23]. GOCI images have been used to monitor the suspended sediment in Taihu Lake [24] and the coastal waters of Zhejiang, China [25], as well as Gyeonggi Bay on the west coast of Korea [26]. Moreover, GOCI also monitors long-term suspended sediment concentration and estimates ocean surface currents hourly [27]. However, using GOCI to monitor the spatiotemporal distribution of typhoon-induced SS in coastal waters has not been considered in previous case studies.

This study used GOCI to monitor the spatial and temporal distribution of SS pre- and post-Typhoon Soudelor, which made landfall in Taiwan in August 2015. Furthermore, by taking advantage of GOCI with time-series hourly images of SS after the typhoon, the temporal decay of the SS pattern can be computed by an exponential regression, and the time SS recovered to its pre-typhoon value can be estimated. This approach, which is the core of the study, quantifies the typhoon-induced spatial and temporal distribution of SS along Taiwan coastal water. Finally, factors such as river discharge and ocean currents could have affected the discussed spatiotemporal distribution of SS.

2. Materials and Methods

2.1. Study Area

The study area is located on the northern coast of Taiwan (Figure 1). There are 9 rivers administered by the Taiwan central government (ATCG) [28]. Seven of the rivers are on the west side of Taiwan Island, and two are on the east side.

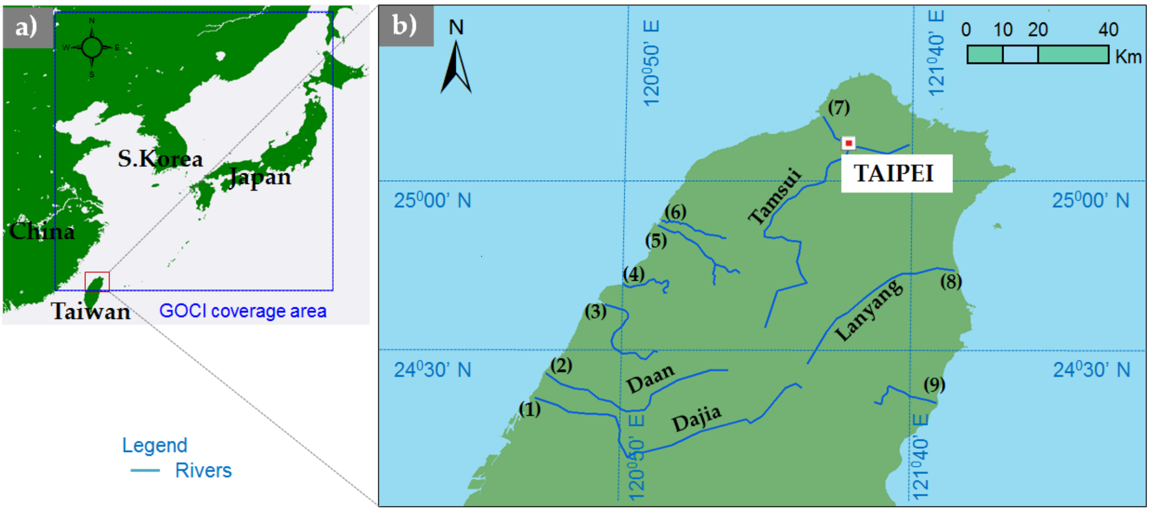

Figure 1. (**a**) Visualization of Geostationary Ocean Color Imager (GOCI) coverage area; (**b**) study area.

The statistics of the annual discharge of the 9 rivers were provided by the Taiwan River Restoration Network [28]. Tamsui River has the largest annual discharge of 7443 m^3/s, followed by Lanyang and Dajia with 2773 m^3/s and 2569 m^3/s, respectively. Other rivers have a lower discharge of less than 2000 m^3/s, and the Fengshan River has the lowest discharge of 376 m^3/s.

2.2. Typhoon Soudelor

Typhoon Soudelor formed in the middle of the Pacific Ocean on 20 July 2015, and became a super typhoon (category 5 on the Saffir–Simpson hurricane wind scale) on 29 July [29]. Typhoon Soudelor made landfall in the east of Taiwan at 04:40 local time on 8 August 2015 and brought torrential rain. The typhoon then moved north-westwards through eastern China and degraded to a tropical depression on 9 August 2015 [30–33].

2.3. GOCI Satellite Images

In this study, GOCI level-2 images were downloaded from the NASA Ocean Color website (https://oceancolor.gsfc.nasa.gov/). Then, SS was extracted from GOCI hourly images with a spatial resolution of 500 m. These hourly images were binned using the arithmetic mean algorithm, implemented in SeaDAS [34,35], to create daily SS images with a spatial resolution of 500 m (Figure 2).

During the period of Typhon Soudelor, cloud cover caused data voids in many of the hourly GOCI images. The problem was more severe on 8–10 and 15–18 August, when GOCI images were not available for our study area (Figure 2). To better visualize the spatial distribution of typhoon-induced SS, i.e., minimize the data voids, 4 daily GOCI images were further binned to generate a 4-day average image with a spatial resolution of 500 m.

A 4-day average image immediately before the typhoon ($\overline{SS}_{4-7}$), binned from the daily SS images of 4–7 August 2015, was generated. Similarly, a 4-day average image immediately after the typhoon ($\overline{SS}_{11-14}$), binned from 11–14 August, was generated. Moreover, to monitor the decrease in suspended sediment, a 4-day average image 9 to 12 days after the typhoon ($\overline{SS}_{19-22}$), binned from the daily SS images of 19–22 August, was generated. Figure 2 shows the data processing of GOCI images in this study.

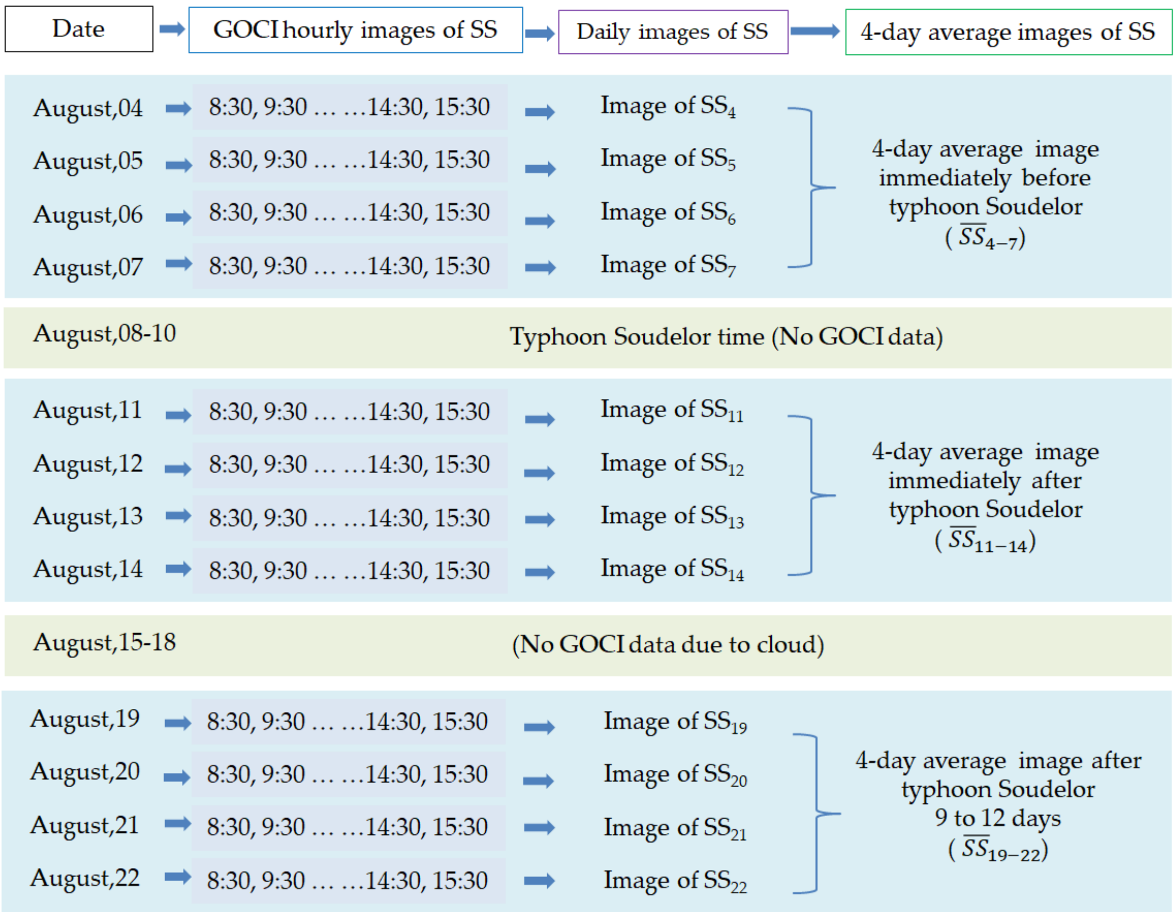

Figure 2. GOCI data processing for generating $\overline{SS}_{4-7}$, $\overline{SS}_{11-14}$, and $\overline{SS}_{19-22}$. SS: suspended sediment.

2.4. *Quantitative Retrieval Algorithm of SS*

In this paper, SS images were derived from level-2 GOCI images by using the algorithm developed by Moon et al. (2010) based on in-situ SS samples (Equation (1)) [20]:

$$SS = 945.07 \times (Rrs(555))^{1.137} \tag{1}$$

where *Rrs* (555) is remote sensing reflectance at a wavelength of 555 nm, and *SS* is reported in g/m^3. The algorithm was implemented in the GOCI Data Processing System (GDPS) by KOSC [36].

2.5. *Temporal Decay of SS after Typhoon*

When showing the temporal history of hourly SS of a GOCI pixel (Figure 3), the maximum SS value (SS_{max}) was reached in a few days, varying with pixel locations, after Typhoon Soudelor made landfall on Taiwan. In this research, SS_{max} of each pixel was determined as the largest hourly SS value of that pixel from 11–22 August. The time when the pixel reaches SS_{max} is denoted as t_{max}.

An interesting feature in the temporal history of SS (Figure 3) is its decaying pattern, where the SS value decreases after t_{max}. We proposed using a decaying model to quantify the pattern by fitting an exponential curve to hourly SS data for each GOCI pixel via regression. It was found (with internal trials) that a robust result of the regression was obtained for GOCI pixels that had more than 5 hourly SS values available after their t_{max}. Figure 3 shows an example of the regression result depicting the decaying exponential model after t_{max}, despite the GOCI pixel not having data from 15 to 18 August due to cloud cover.

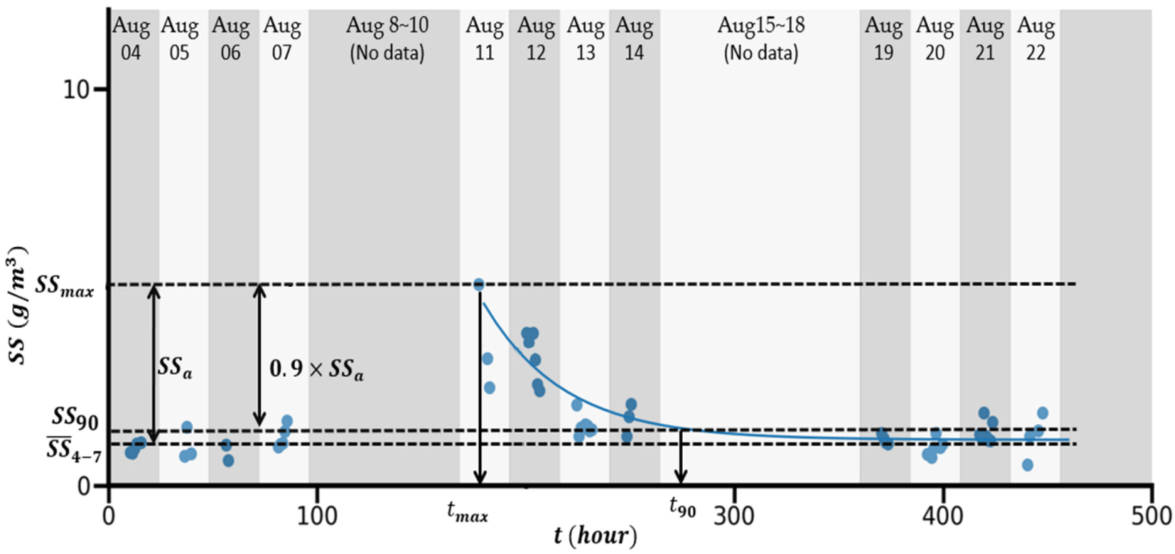

Figure 3. Example of temporal decay of suspended sediment (SS). Corresponding SS_{90} with t_{90} are denoted.

Ideally, taking advantage of this decaying model, the time for the pixel to return to its pre-typhoon state could be estimated using the regression result. However, it was found that the decaying exponential model of many GOCI pixels only approaches the pre-typhoon state asymptotically, i.e., the regression line shown in Figure 3 does not intersect with $\overline{SS}_{4-7}$. Instead, we demonstrate the use of this model by computing dissipation of 90% increased SS. This would fit for the application of coastal ecology management, as the ecosystem is resilient to a certain increase in SS for a short period of time.

The amount of increased SS, denoted as SS_a, for each GOCI pixel, can be computed as

$$SS_a = SS_{max} - \overline{SS}_{4-7} \tag{2}$$

and SS_{90}, which represents 90% of SS_a, is dissipated from its maximum value (Figure 3).

$$SS_{90} = SS_{max} - 0.9 \times SS_a \tag{3}$$

Furthermore, the time corresponding to SS_{90} can be identified via the regressed exponential decay and is denoted as t_{90} (Figure 3).

3. Results

3.1. Spatial–Temporal Analysis of SS Pre- and Post-Typhoon Soudelor

During the pre-typhoon period ($\overline{SS}_{4-7}$ in Figure 4a), SS with a concentration of 3–6 g/m^3 was mainly distributed along the west coastal water. The mouths of both the Dajia River and Tamsui River had an SS greater than 6 g/m^3. The SS concentration in the east coastal water was less than 3 g/m^3.

During the post-typhoon period of 11–14 August ($\overline{SS}_{11-14}$ in Figure 4b), the SS of the Taiwan coastal water generally increased. The SS along the west and east coastal waters increased to values greater than 6 and 3 g/m^3, respectively. Meanwhile, the mouths of the Dajia River and Tamsui River (west coastal water) had SS values greater than 9 g/m^3 and the Lanyang River mouth (east coastal water) had an SS value greater than 6 g/m^3.

During the post-typhoon period of 19–22 August ($\overline{SS}_{19-22}$ in Figure 4c), the general distribution of SS along the west coastal water was similar to that of the pre-typhoon period (Figure 5a), except for the mouths of the Dajia River and Tamsui River having an SS value greater than 9 g/m^3. A belt with relatively high SS values (greater than 3 g/m^3) was found along the east coastal water with a width of approximately 3 km. In addition, the mouths of both the Lanyang River and Heping River had SS values greater than 6 g/m^3.

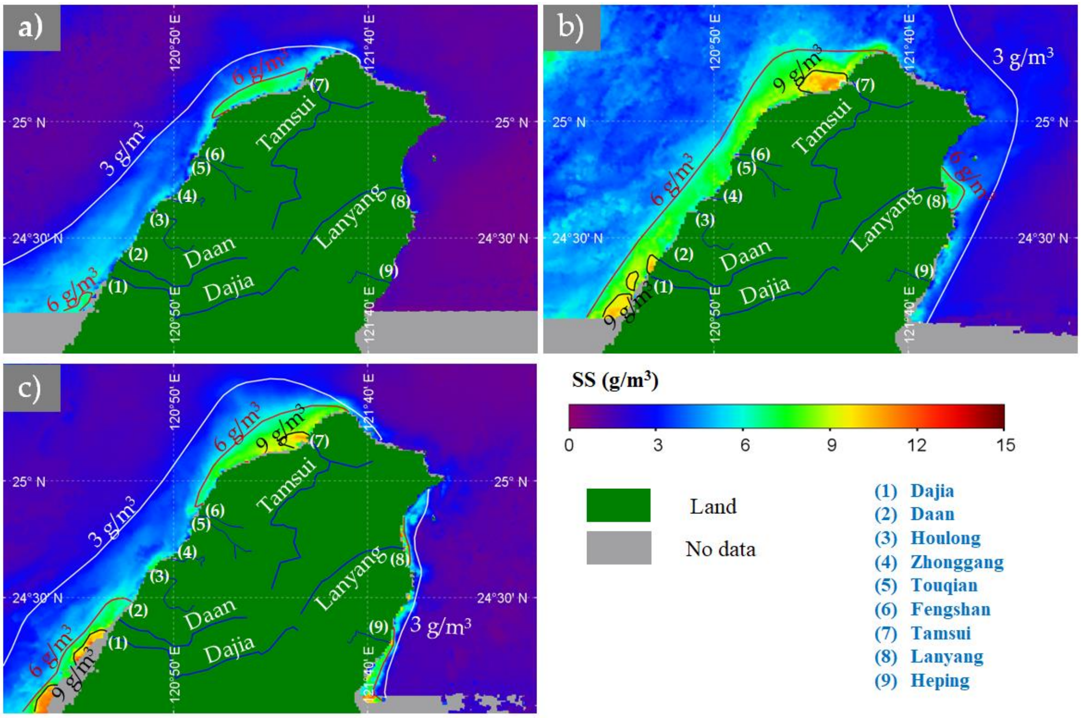

Figure 4. Spatial distribution of SS pre- and post-typhoon: (**a**) $\overline{SS}_{4-7}$; (**b**) $\overline{SS}_{11-14}$; (**c**) $\overline{SS}_{19-22}$.

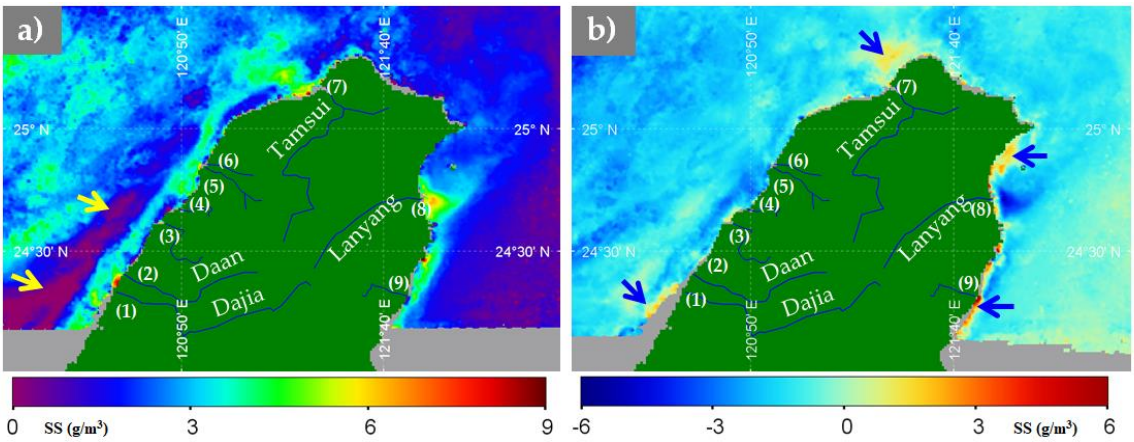

Figure 5. Temporal difference of SS: (**a**) $\overline{SS}_{11-14} - \overline{SS}_{4-7}$; (**b**) $\overline{SS}_{19-22} - \overline{SS}_{11-14}$.

Comparing the SS between the post-typhoon period of 11–14 August ($\overline{SS}_{11-14}$) and pre-typhoon ($\overline{SS}_{4-7}$), it was found that all pixels increased more than 1 g/m^3 (Figure 5a), except for a tongue-shaped area (denoted by arrows in Figure 5a) located 10–20 km off the west coastal water of Taiwan. In addition, the distribution of increased SS showed prominent heterogeneity along the coastal water of Taiwan. A high increase in SS (i.e., greater than 6.0 g/m^3) was found at the mouths of the Dajia, Daan, Tamsui, and Lanyang Rivers. Three regions with a low SS increase (less than 2 g/m^3) along the coast, from the Daan River mouth to Zhonggan River mouth, the Fengshan River mouth to Tamsui River mouth, and the Tamsui River to Lanyang River mouth, were also identified (Figure 5a).

Comparing the SS between two post-typhoon periods of 19–12 August ($\overline{SS}_{19-22}$) and 11–14 August ($\overline{SS}_{11-14}$), it was found that most of the pixels decreased while some remained with increased SS values (Figure 5b). Most of the pixels decreased to less than 3 g/m^3. The Lanyang River mouth showed the most significant decrease of 6 g/m^3, followed by the Zhonggang and Tauqian River mouths, with a reduction of 3 g/m^3. In contrast, the Dajia River mouth showed an increased SS value greater than 3 g/m^3 and the Heping

River mouth showed an increased SS value of 6 g/m^3. It is also interesting to note that neighboring regions with increased SS (greater than 3 g/m^3) were found northeast of the Tamsui River mouth and north of the Lanyang River mouth. The regions with increased SS are indicated by arrows in Figure 5b.

With the GOCI average SS data, it was observed that SS in the west coastal water was consistently greater than that on the east coastal water regardless of the effect of Typhoon Soudelor. In addition, hotspots of high SS value (greater than 9 g/m^3) were found at the Dajia and Tamsui River mouth in the two post-typhoon periods ($\overline{SS}_{11-14}$ and $\overline{SS}_{19-22}$). With the GOCI data for pre-typhoon ($\overline{SS}_{4-7}$) and post-typhoon ($\overline{SS}_{11-14}$), it was observed that the Taiwan coastal water showed a prominent increase in SS induced by Typhoon Soudelor.

3.2. SS_{max} and t_{max}

Figure 6a shows a visualization of the maximum suspended sediment (SS_{max}) for each GOCI pixel of Taiwan coastal water during the post-typhoon period (from 08:30 on 11 August to 15:30 on 22 August). Figure 6b shows its corresponding time (t_{max}) derived from GOCI hourly data.

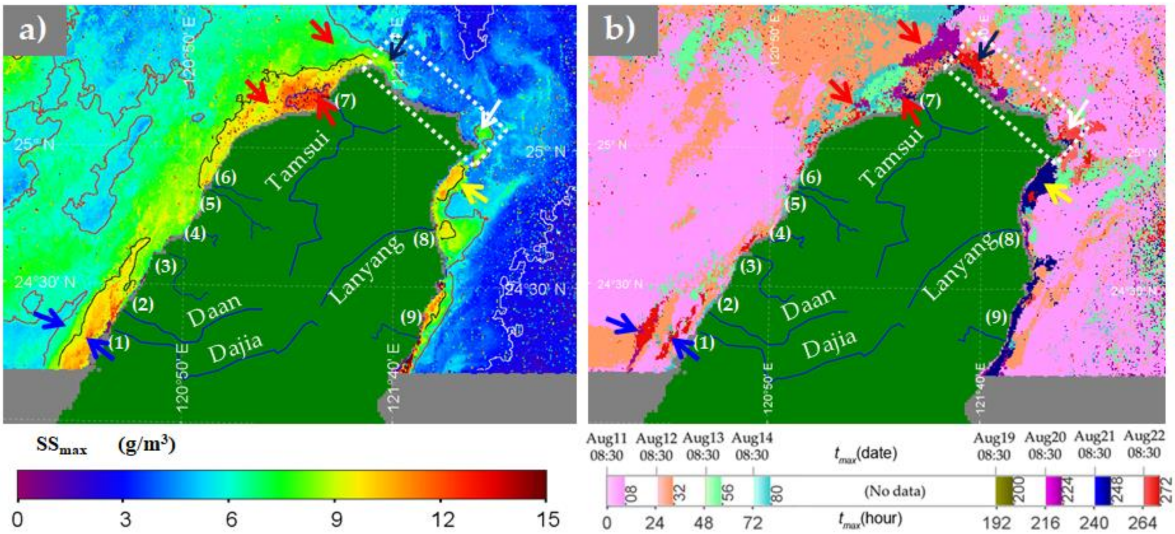

Figure 6. (**a**) Maximum suspended sediment (SS_{max}); (**b**) its corresponding time (t_{max}).

Generally, the west coastal water from the Dajia River mouth to the Tamsui River mouth showed SS_{max} in the range of 9–15 g/m^3 with a corresponding t_{max} of 0–80 h (Figure 6b). This indicates that most of the west coastal water reached SS_{max} during the post-typhoon period of 11–14 August (within four days after Typhoon Soudelor). The exceptions were two strips with t_{max} greater than 264 h located 5 and 15 km away from the Dajia River mouth (denoted by blue arrows in Figure 6b), and three regions with t_{max} greater than 216 h located near the Tamsui River mouth (denoted by red arrows in Figure 6b). Further small regions with t_{max} greater than 264 h sporadically occurred in the coastal water from the Houlong River mouth to Zhonggang River mouth and the Feshang River mouth to Tamsui River mouth.

It is interesting to note that the general appearance of the SS_{max} of the northeast coastal water (indicated by the dotted white rectangle) was lower than the west and east coastal waters, with a range of less than 6 g/m^3, while its t_{max} value showed a large variation of 0–272 h. Most of the coastal water of the northern coast had SS_{max} values in the range of 3–6 g/m^3 with t_{max} of 24–80 h (within four days after Typhoon Soudelor). At the west and east ends (indicated by black and white arrows, respectively, in Figure 6) of the northeast coast, SS_{max} was in the range of 6–9 g/m^3 with a corresponding t_{max} greater than 264 h. It also indicates that both SS_{max} and t_{max} of the northern coastal waters are continuous data from the west and east coastal water. Even though there are no ATCG rivers in this region, SS_{max} and t_{max} have been linked to river-derived suspended sediment.

The east coastal water generally took a long time to reach SS_{max}, with a range of 9–15 g/m^3 compared to the west and northeast coastal waters, with t_{max} of 192–272 h (9–12 days after Typhoon Soudelor). The exception is the coastal water near the Lanyang River mouth, which reached an SS_{max} with t_{max} of 24–80 h (within 4 days after the typhoon). The coastal water near Heping River mouth showed SS_{max} with a range of 6–15 g/m^3 corresponding to t_{max} greater than 240 h (11–12 days after the typhoon). Interestingly, a region north of the Lanyang River mouth (indicated by yellow arrows) also showed a local high SS_{max} of 9–15 g/m^3 with a corresponding t_{max} value similar to the Heping River mouth.

3.3. SS_{90} and t_{90}

Figure 7a shows a visualization of SS_{90}, which means 90% of increasing SS dissipated from its maximum value for each GOCI pixel of Taiwan coastal water. Figure 7b shows the corresponding time (t_{90}) via regressed exponential decay.

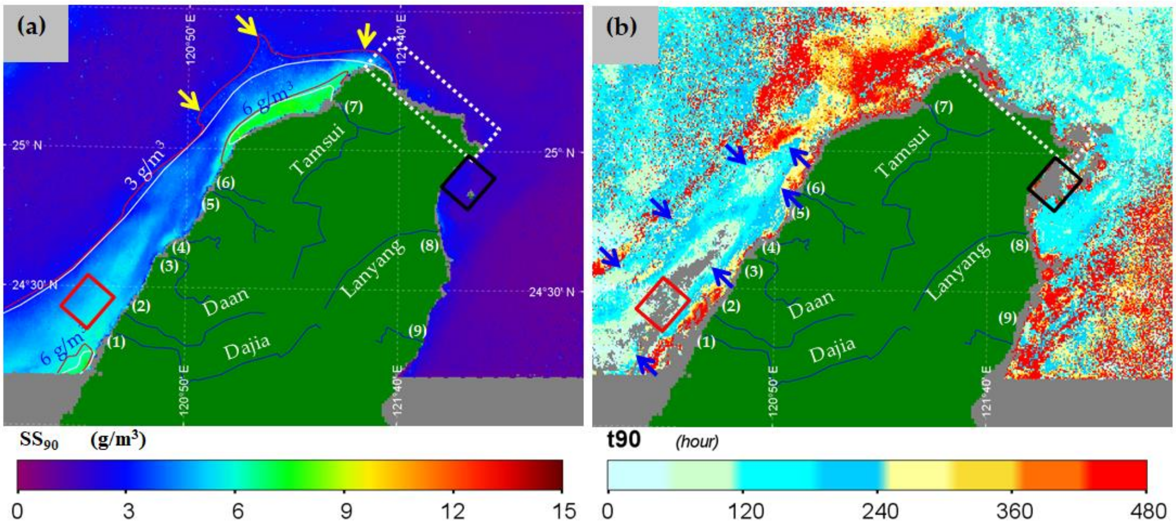

Figure 7. (**a**) SS concentration of each pixel reduced to 90% after typhoon-induced impact; (**b**) its corresponding time t_{90}. White contour lines indicate $\overline{SS}_{4-7}$; red contour lines indicate SS_{90}.

The comparison between SS_{90} (Figure 7a) and $\overline{SS}_{4-7}$ (Figure 4a) indicates that SS_{90} was similar to the pre-typhoon state ($\overline{SS}_{4-7}$), except for the SS of the Tamsui River mouth (within 3–6 g/m^3; indicated by arrows in Figure 7a). Particularly, SS within 3–6 g/m^3 was observed mainly in the west coastal water, while it was less than 3 g/m^3 in the east coastal waters; SS greater than 6 g/m^3 also only appeared at the Tamsui and Dajia River mouths (Figures 7a and 4a). There was a slight difference in SS located 40 km off the Tamsui River mouth. SS_{90} showed that the SS of 3 g/m^3 extended farther into the sea than in $\overline{SS}_{4-7}$.

The west coastal waters from the Dajia River mouth to the Tamsui River mouth showed a t_{90} of more than 240 h, except for a tongue-shaped area with a range of 10–40 km off the west coastal water (indicated by arrows in Figure 7b), showing a t_{90} of less than 240 h. The Tamsui River mouth extending within 20 km of the coastline indicated a t_{90} with a range of 240–480 h.

The northeast coastal water to the Lanyang River mouth (Figure 7a) showed an SS_{90} associated with a t_{90} of less than 240 h, except for small scattered regions that appeared closest to the coastline with a t_{90} of around 480 h (Figure 7b). Lastly, the east coastal waters from the Lanyang to Heping River mouth showed a t_{90} of 360–480 h (Figure 7b).

It should be noted that some pixels available in the SS_{90} are not visualized by the t_{90}. There are two cases in which the decaying model works without advantages, leading to the pixel in t_{90} not being visualized. When GOCI pixels (indicated by a red rectangle in Figure 7) have a gap between SS_{max} and $\overline{SS}_{4-7}$, which is close (Figure 3), t_{90} is not visualized due to no decay. When the number of GOCI pixels after t_{max} has fewer than five values, it is also not visualized because of the lack of data (indicated by the black rectangle in Figure 7). Otherwise, the proposed methodology, which uses an exponential temporal decaying model, shows a distinct advantage when GOCI pixels have more than five hourly SS values available after their t_{max}. It is possible to compute the t_{90} with robust results post-typhoon.

4. Discussion

According to previous studies in Taiwan, one possible reason for the SS derived from a typhoon is that it is strongly affected by river discharge. For example, using a case study in Choshui River, Taiwan, and Typhoon Mindulle, the authors of [37] indicated that in a floodplain, more than half of the suspended sediment originating from mountain rivers running into Taiwan coastal waters was generated by river discharge. The authors of [38] observed the Jhoushui River and an adjacent coastal zone in the Taiwan Strait and summarized that the river discharges most of the sediment during the relatively short periods of torrential rain often associated with typhoons. Moreover, the authors of [39,40] indicated that suspended sediment discharge during typhoon events was linked to landslides and rainfall in Taiwan. The authors of [41] considered the impact of typhoons on sediment discharge in Taiwan. River discharge also impacted the change in sediment concentration in the Tamsui River, as discussed in [42]. Even though we have the same opinion, there are no recorded data to support the Typhoon Soudelor case. Therefore, examining the mechanical factors, such as river discharge, related to typhoons is beyond the scope of this study. We only discuss this based on the mean annual discharge data, which were provided by the Taiwan River Restoration Network [28,43].

In terms of the mean annual discharge related to the nine central rivers administered by ATCG, the Tamsui River supplies the largest amount with 7443 m^3/s, followed by the Lanyang and Dajia Rivers with 2773 and 2596 m^3/s, respectively. This is the reason why the Tamsui, Dajia, and Lanyang River mouths act as hotspots with high SS values (SS_{max} above 9 g/m^3) during the two post-typhoon periods ($\overline{SS}_{11-14}$ and $\overline{SS}_{19-22}$). Meanwhile, other rivers show a mean annual discharge lower than 2000 m^3/s, and they influence the coastal regions with SS_{max} values in the range of 6–9 g/m^3. The central rivers are mainly located in the western part of Taiwan, which may be why many GOCI pixels of the west coastal waters are more influenced than those of the east coastal waters, regardless of the effect of Typhoon Soudelor.

Other factors such as tide level, waves, wind speed, and surface currents that impact the spatiotemporal distribution of SS should also be discussed. All of these factors have been considered by many scientists. According to the authors of [44], by using shipboard observations for estimation, transport and tidal currents in the Taiwan Strait were northward (into the East China Sea). This is similar to the ocean surface current from GOCI satellite imagery in summer around the north of Taiwan coastal water being northward [45]. Therefore, we also believe that after Typhoon Soudelor, the ocean surface was a major factor in increasing the outbreak of suspended sediment north of Taiwan. However, due to the limitation of recorded data on Typhoon Soudelor, the transport mechanism responsible for the sediment warrants further investigation.

5. Conclusions

This paper proposes a new approach using the GOCI to monitor the spatial and temporal distribution of suspended sediment in coastal areas affected by typhoons. Remote sensing technology was used instead of other methods such as in situ measurements, numerical models, and station observations to track post-typhoon sediment concentration in Taiwan coastal waters.

The spatial distribution of SS has been highlighted by using the GOCI four-day average image of SS pre- and post-Typhoon Soudelor. As a result, several pixels with an SS above 6 g/m^3 in the west coastal waters were consistently more significant than in the east coastal waters regardless of the typhoon. The Dajia and Tamsui River mouths were hotspots of increased SS and SS_{max} (above 9 g/m^3) during two post-typhoon periods (11–14 and 29–22 August).

According to the GOCI hourly data after the typhoon, SS_{max} was in the range of 6–15 g/m^3, corresponding to t_{max} within four days in the west coastal water, while the east coastal water was 9–12 days. Furthermore, using exponential regression decay to visualize SS_{90} for each GOCI pixel in Taiwan coastal water indicates that SS_{90} was in an asymptotic pre-typhoon state. The corresponding time t_{90} shows that GOCI pixels in both the Tamsui and Heping River mouths generally took the longest time, in a range of 360–480 h.

River discharge could have a significant impact on the post-typhoon sediment characteristics of Taiwan coastal waters. Other factors such as tide level, waves, wind speed, and surface currents could also affect the spatiotemporal distribution of suspended sediment. We suggest that this should be investigated in the future by using a successfully recorded dataset with a new typhoon.

Author Contributions: Conceptualization, C.-K.W.; Data curation, P.M.C.; Formal analysis, P.M.C.; Investigation, P.M.C.; Methodology, P.M.C., C.-K.W. and A.-T.H.; Project administration, C.-K.W.; Software, A.-T.H.; Supervision, C.-K.W.; Validation, P.M.C.; Visualization, P.M.C. and A.-T.H.; Writing—original draft, P.M.C. and A.-T.H.; Writing—review & editing, C.-K.W. All authors have read and agreed to the published version of the manuscript.

Funding: The APC was supported in part by Higher Education Sprout Project, Ministry of Education to the Headquarters of University Advancement at National Cheng Kung University (NCKU).

Institutional Review Board Statement: Not applicable.

Informed Consent Statement: Not applicable.

Data Availability Statement: The data that support the findings of this study are available from the corresponding author upon reasonable request.

Acknowledgments: The authors thank NASA for providing free GOCI satellite images and the SeaDAS application. We also thank the Korea Ocean Satellite Center for providing the GDPS application. The authors would also like to thank the Taiwan River Restoration Network for sharing river system information. Finally, the authors deeply acknowledge anonymous reviewers for their constructive comments and suggestion toward improving this manuscript.

Conflicts of Interest: The authors declare no conflict of interest.

References

1. Snelgrove, P.V.R.; Henry Blackburn, T.; Hutchings, P.A.; Alongi, D.M.; Frederick Grassle, J.; Hummel, H.; King, G.; Koike, I.; Lambshead, P.J.D.; Ramsing, N.B.; et al. The importance of marine sediment biodiversity in ecosystem processes. *Ambio* **1997**, *26*, 578–583.
2. Ouillon, S. Why and how do we study sediment transport? Focus on coastal zones and ongoing methods. *Water* **2018**, *10*, 390. [CrossRef]
3. Casal, G.; Harris, P.; Monteys, X.; Hedley, J.; Cahalane, C.; Casal, G.; Harris, P.; Monteys, X.; Hedley, J.; Cahalane, C.; et al. Understanding satellite-derived bathymetry using Sentinel 2 imagery and spatial prediction models. *GIScience Remote Sens.* **2020**, *57*, 271–286. [CrossRef]
4. Volpe, V.; Silvestri, S.; Marani, M. Remote sensing retrieval of suspended sediment concentration in shallow waters. *Remote Sens. Environ.* **2011**, *115*, 44–54. [CrossRef]
5. Ody, A.; Doxaran, D.; Vanhellemont, Q.; Nechad, B.; Novoa, S.; Many, G.; Bourrin, F.; Verney, R.; Pairaud, I.; Gentili, B. Potential of high spatial and temporal ocean color satellite data to study the dynamics of suspended particles in a micro-tidal river plume. *Remote Sens.* **2016**, *8*, 245. [CrossRef]
6. Malenovský, Z.; Rott, H.; Cihlar, J.; Schaepman, M.E.; García-Santos, G.; Fernandes, R.; Berger, M. Sentinels for science: Potential of Sentinel-1, -2, and -3 missions for scientific observations of ocean, cryosphere, and land. *Remote Sens. Environ.* **2012**, *120*, 91–101. [CrossRef]

7. Li, Y.; Li, D.; Fang, J.; Yin, X.; Li, H.; Hu, W.; Chen, J. Impact of Typhoon Morakot on suspended matter size distributions on the East China Sea inner shelf. *Cont. Shelf Res.* **2015**, *101*, 47–58. [CrossRef]
8. He, X.; Bai, Y.; Chen, C.-T.A.; Hsin, Y.-C.; Wu, C.-R.; Zhai, W.; Liu, Z.; Gong, F. Satellite views of the episodic terrestrial material transport to the southern Okinawa Trough driven by typhoon. *J. Geophys. Res. Ocean.* **2014**, *119*, 1706–1722. [CrossRef]
9. Liu, J.; Cai, S.; Wang, S. Observations of strong near-bottom current after the passage of Typhoon Pabuk in the South China Sea. *J. Mar. Syst.* **2011**, *87*, 102–108. [CrossRef]
10. Miles, T.; Seroka, G.; Kohut, J.; Schofield, O.; Glenn, S. Glider observations and modeling of sediment transport in Hurricane Sandy. *J. Geophys. Res. Ocean.* **2015**, *120*, 1771–1791. [CrossRef]
11. Li, Y.; Wang, A.; Qiao, L.; Fang, J.; Chen, J. The impact of typhoon Morakot on the modern sedimentary environment of the mud deposition center off the Zhejiang-Fujian coast, China. *Cont. Shelf Res.* **2012**, *37*, 92–100. [CrossRef]
12. Li, Y.; Li, H.; Qiao, L.; Xu, Y.; Yin, X.; He, J. Storm deposition layer on the Fujian coast generated by Typhoon Saola (2012). *Sci. Rep.* **2015**, *5*, 1–7. [CrossRef]
13. Chen, S.; Huang, W.; Wang, H.; Li, D. Remote sensing assessment of sediment re-suspension during Hurricane Frances in Apalachicola Bay, USA. *Remote Sens. Environ.* **2009**, *113*, 2670–2681. [CrossRef]
14. Li, Y.; Li, X. Remote sensing observations and numerical studies of a super typhoon-induce d suspende d se diment concentration variation in the East China Sea. *Ocean Model.* **2016**, *104*, 187–202. [CrossRef]
15. Doxaran, D.; Lamquin, N.; Park, Y.J.; Mazeran, C.; Ryu, J.H.; Wang, M.; Poteau, A. Retrieval of the seawater reflectance for suspended solids monitoring in the East China Sea using MODIS, MERIS and GOCI satellite data. *Remote Sens. Environ.* **2014**, *146*, 36–48. [CrossRef]
16. Li, Y.; Xu, X.; Yin, X.; Fang, J.; Hu, W.; Chen, J. Remote-sensing observations of Typhoon Soulik (2013) forced upwelling and sediment transport enhancement in the northern Taiwan Strait. *Int. J. Remote Sens.* **2015**, *36*, 2201–2218. [CrossRef]
17. Li, Y.; Xu, X.; Zheng, B. Satellite views of cross-strait sediment transport in the Taiwan Strait driven by Typhoon Morakot (2009). *Cont. Shelf Res.* **2018**, *166*, 54–64. [CrossRef]
18. Choi, J.K.; Park, Y.J.; Ahn, J.H.; Lim, H.S.; Eom, J.; Ryu, J.H. GOCI, the world's first geostationary ocean color observation satellite, for the monitoring of temporal variability in coastal water turbidity. *J. Geophys. Res. Ocean.* **2012**, *117*, 1–10. [CrossRef]
19. Choi, J.-K.; Park, Y.J.; Lee, B.R.; Eom, J.; Moon, J.-E.; Ryu, J.-H. Application of the Geostationary Ocean Color Imager (GOCI) to mapping the temporal dynamics of coastal water turbidity. *Remote Sens. Environ.* **2014**, *146*, 24–35. [CrossRef]
20. Moon, J.-E.; Ahn, Y.-H.; Ryu, J.-H.; Shanmugam, P. Development of Ocean Environmental Algorithms for Geostationary Ocean Color Imager (GOCI). *Korean J. Remote Sens.* **2010**, *26*, 189–207.
21. Ryu, J.H.; Han, H.J.; Cho, S.; Park, Y.J.; Ahn, Y.H. Overview of geostationary ocean color imager (GOCI) and GOCI data processing system (GDPS). *Ocean Sci. J.* **2012**, *47*, 223–233. [CrossRef]
22. Moon, J.E.; Park, Y.J.; Ryu, J.H.; Choi, J.K.; Ahn, J.H.; Min, J.E.; Son, Y.B.; Lee, S.J.; Han, H.J.; Ahn, Y.H. Initial validation of GOCI water products against in situ data collected around Korean peninsula for 2010–2011. *Ocean Sci. J.* **2012**, *47*, 261–277. [CrossRef]
23. Cheng, Z.; Wang, X.H.; Paull, D.; Gao, J. Application of the Geostationary Ocean Color Imager to mapping the diurnal and seasonal variability of surface suspended matter in a macro-tidal estuary. *Remote Sens.* **2016**, *8*, 244. [CrossRef]
24. Huang, C.; Yang, H.; Zhu, A.X.; Zhang, M.; Lü, H.; Huang, T.; Zou, J.; Li, Y. Evaluation of the Geostationary Ocean Color Imager (GOCI) to monitor the dynamic characteristics of suspension sediment in Taihu Lake. *Int. J. Remote Sens.* **2015**, *36*, 3859–3874. [CrossRef]
25. Qiu, Z.; Zheng, L.; Zhou, Y.; Sun, D.; Wang, S.; Wu, W. Innovative GOCI algorithm to derive turbidity in highly turbid waters: A case study in the Zhejiang coastal area. *Opt. Express* **2015**, *23*, A1179. [CrossRef]
26. Choi, J.-K.; Yang, H.; Han, H.-J.; Ryu, J.-H.; Park, Y.-J. Quantitative estimation of suspended sediment movements in coastal region using GOCI. *J. Coast. Res.* **2013**, *165*, 1367–1372. [CrossRef]
27. Yang, H.; Choi, J.-K.; Park, Y.-J.; Han, H.-J.; Ryu, J.-H. Application of the Geostationary Ocean Color Imager (GOCI) to estimates of ocean surface currents. *J. Geophys. Res. Ocean.* **2014**, 1022–1037. [CrossRef]
28. Taiwan River Restotation Network the List of Central Rivers. Available online: http://trrn.wra.gov.tw/web/index-18.html (accessed on 26 April 2020).
29. National Hurricane Centre Saffir-Simpson Hurricane Wind Scale. *Wind Scale* **2012**, 1–2. Available online: http://www.nhc.noaa.gov/aboutsshws.php (accessed on 15 May 2020).
30. Chen, W.B.; Lin, L.Y.; Jang, J.H.; Chang, C.H. Simulation of typhoon-induced storm tides and wind waves for the northeastern coast of Taiwan using a tide-surge-wave coupled model. *Water* **2017**, *9*, 549. [CrossRef]
31. Typhoon Taiwan's Typhoon Data Base. Available online: http://rdc28.cwb.gov.tw/TDB/ntdb/pageControl/typhoon?year=2015&num=201513&name=SOUDELOR&from_warning=tru (accessed on 31 March 2018).
32. Soudelor Typhoon Soudelor Wiki. Available online: https://en.wikipedia.org/wiki/Typhoon_Soudelor (accessed on 24 April 2018).
33. Soudelor, T. Deadly Typhoon Soudelor's Rainfall Analyzed. Available online: https://pmm.nasa.gov/extreme-weather/deadly-typhoon-soudelors-rainfall-analyzed (accessed on 1 July 2020).
34. Brockmann Consult L3/Binning Tool. Available online: http://www.brockmann-consult.de/beam/doc/help-4.8/binning/BinningAlgorithmDescription.html (accessed on 11 November 2018).

35. Campbell, J.W.; Blaisdell, J.M.; Darzi, M. Level-3 SeaWiFS Data Products: Spatial and Temporal Binning Algorithms. *SeaWiFS Tech. Rep. Ser.* **1995**, *32*, 80.
36. Technologies, M. GDPS Ver.2.0 User's Manual. 2018. Available online: http://kosc.kiost.ac.kr/eng/p30/kosc_p34.html (accessed on 10 November 2018).
37. Milliman, J.D.; Lee, T.Y.; Huang, J.C.; Kao, S.J. Temporal and spatial responses of river discharge to tectonic and climatic perturbations: Choshui River, Taiwan, and Typhoon Mindulle (2004). *Proc. Int. Assoc. Hydrol. Sci.* **2015**, *29*, 11–14. [CrossRef]
38. Chien, H.; Chiang, W.S.; Kao, S.J.; Liu, J.T.; Liu, K.K.; Liu, P.L.F. Sediment Dynamics observed in the Jhoushuei River and Adjacent Coastal Zone in Taiwan Strait. *Oceanography* **2011**, *24*, 122–131. [CrossRef]
39. Lin, G.W.; Chen, H.; Chen, Y.H.; Horng, M.J. Influence of typhoons and earthquakes on rainfall-induced landslides and suspended sediments discharge. *Eng. Geol.* **2008**, *97*, 32–41. [CrossRef]
40. Chen, C.W.; Oguchi, T.; Hayakawa, Y.S.; Saito, H.; Chen, H.; Lin, G.W.; Wei, L.W.; Chao, Y.C. Sediment yield during typhoon events in relation to landslides, rainfall, and catchment areas in Taiwan. *Geomorphology* **2018**, *303*, 540–548. [CrossRef]
41. Hung, C.; Lin, G.-W.; Kuo, H.-L.; Zhang, J.-M.; Chen, C.-W.; Chen, H. Impact of an Extreme Typhoon Event on Subsequent Sediment Discharges and Rainfall-Driven Landslides in Affected Mountainous Regions of Taiwan. *Geofluids* **2018**, *2018*, 1–11. [CrossRef]
42. Liu, W.C.; Chen, W.B.; Cheng, R.T.; Hsu, M.H. Modelling the impact of wind stress and river discharge on Danshuei River plume. *Appl. Math. Model.* **2008**, *32*, 1255–1280. [CrossRef]
43. Water Resources Planning Institute, Water Resources Agency, Ministry of Economic Affairs. Available online: https://www.wrap.gov.tw/pro12.aspx?type=0201000000 (accessed on 23 March 2020). (In Chinese)
44. Wang, Y.H.; Jan, S.; Wang, D.P. Transports and tidal current estimates in the Taiwan Strait from shipboard ADCP observations (1999–2001). *Estuar. Coast. Shelf Sci.* **2003**, *57*, 193–199. [CrossRef]
45. Liu, J.; Emery, W.; Wu, X.; Li, M.; Li, C.; Zhang, L. Computing Coastal Ocean Surface Currents from MODIS and VIIRS Satellite Imagery. *Remote Sens.* **2017**, *9*, 1083. [CrossRef]